Facilitating URLLC vis-à-vis UAV-enabled relaying for MEC Systems in 6G Networks

Ali Ranjha, Diala Naboulsi, Mohamed El Emary, Francois Gagnon

Facilitating URLLC vis-à-vis UAV-enabled relaying for MEC Systems in 6G Networks

Ali Ranjha, Diala Naboulsi, *Member, IEEE*, Mohamed El Emary, and Francois Gagnon, *Senior Member, IEEE*

***Abstract*—The futuristic sixth-generation (6G) networks will empower ultra-reliable and low latency communications (URLLC), enabling a wide array of mission-critical applications such as mobile edge computing (MEC) systems, which are largely unsupported by fixed communication infrastructure. To remedy this issue, unmanned aerial vehicle (UAV) has recently come to the limelight to facilitate MEC for internet of things (IoT) devices as they provide desirable line-of-sight (LoS) communications compared to fixed terrestrial networks, thanks to their added flexibility and three-dimensional (3D) positioning. In this paper, we consider UAV-enabled relaying for MEC systems for uplink transmissions in 6G networks, and we aim to optimize mission completion time subject to the constraints of resource allocation, including UAV transmit power, UAV CPU frequency, decoding error rate, blocklength, communication bandwidth, and task partitioning as well as 3D UAV positioning. Moreover, to solve the non-convex optimization problem, we propose three different algorithms, including successive convex approximations (SCA), altered genetic algorithm (AGA) and smart exhaustive search (SES). Thereafter, based on time-complexity, execution time, and convergence analysis, we select AGA to solve the given optimization problem. Simulation results demonstrate that the proposed algorithm can successfully minimize the mission completion time, perform power allocation at the UAV side to mitigate information leakage and eavesdropping as well as map a 3D UAV positioning, yielding better results compared to the fixed benchmark sub-methods. Lastly, subject to 3D UAV positioning, AGA can also effectively reduce the decoding error rate for supporting URLLC services.**

***Index Terms*—URLLC, UAV-enabled relaying, MEC systems, 6G networks.**

I. Introduction

With the emergence of internet-of-things (IoT) and the demand for new service types in the present fifth-generation (5G) and futuristic sixth-generation (6G) networks security and reliability have become the two main concerns for these networks. To this end, in [1], the authors studied security of data in 6G IoT networks by leveraging an ant colony optimization (ACO) approach. As such, the authors utilized the prelarge concept to reduce multiple database scans in the evaluation process and maintained Pareto solutions to improve the optimized results. In the recent years, the mobile operators have witnessed a paradigm shift from centralized to edge computing. Consequently, there are traditional fixed edge computing systems at the base stations (BSs) and alternatively there are mobile edge computing (MEC) systems. In this context, in [2], the authors proposed the framework of digital twinning (DT)-empowered internet of vehicles (IoV) and studied a multi-user offloading system to edge computing, where quality-of-service (QoS) is analyzed through response time of services. In this regard, the authors leveraged a service offloading (SOL) method coupled with deep reinforcement learning for the proposed DT-empowered IoV. Among these two types of edge computing systems, MEC has emerged as a suitable candidate aiming to bring computation capabilities at the networks' edge with two distinctive properties of having proximity to the ground users as well as geographically flexible deployment [3]. Thus, MEC has added degree of freedom and can maintain high QoS for the end users.

A. Background

In this context, the 6G networks are intended to support ultra-reliable and low-latency communications (URLLC) services. Moreover, the short blocklength URLLC packets have dual preconditions of ultra-high reliability and low-latency, which are closely correlated with each other. This QoS requirement of ultra-high reliability can be 10^{-7} or less depending on the mission-critical application-type. Consequently, URLLC systems utilize a short blocklength equation accounting for non-negligible decoding error rate and channel variability, which is fundamentally a penalized version of Shannon's capacity. These days UAVs have become well-known due to their versatility and low cost helping them to find their applications and foothold in various domains of public, civil, and military interests [4]–[9]. It is worth mentioning that for fixed communication infrastructure BSs are placed based on the statistical flow of the cellular traffic. As such these terrestrial networks fail to accommodate a rapid communication traffic increase that can occur in areas that have been struck by natural disasters or during seasonal sporting events or music festivals. To address these problems, UAVs can establish the desirable line-of-sight (LoS) communications to provide higher signal-to-noise ratios (SNRs) owing to their adjustable three-dimensional (3D) positioning, which is a clear advantage over fixed terrestrial networks [10]–[12].

B. Related Works

Recently, the research on UAV-enabled communications, where UAV acts as a flying BS or an aerial relay has gained a significant traction as mentioned in [13]–[17]. In [13], the authors made use of a practical scenario for taking the

A. Ranjha, D. Naboulsi, and M. El Emary are with the Department of Software Engineering and IT, École de Technologie Supérieure, Montréal, QC, H3C 1K3, CA, (e-mails: ali-nawaz.ranjha.1@ens.estmtl.ca, diala.naboulsi@etsmtl.ca, mohamed-ibrahim-mahmoud.el-emary.1@ens.etsmtl.ca).
F. Gagnon is with the Department of Electrical Engineering, École de Technologie Supérieure, Montréal, QC, H3C 1K3, CA, (e-mail: francois.gagnon@etsmtl.ca).

TABLE I: Summary of symbols and descriptions

Symbols	Descriptions
$\mathbf{h}_k$	IoT-UAV channel
d_k^2	Distance existing between each IoT device k and the UAV
g_k	Rician fading
h_r	UAV-AP channel
d_r^2	Distance existing between the UAV and the remote AP
P_k	Transmit power for task offloading
$R_k^{(0)}$	Data rate for sending IoT device k tasks
$R_k^{(2)}$	Data rate for sending IoT device k sub-task from the UAV to the remote AP
T	Mission completion time
F_{max}	Maximum CPU frequency
L_k	Task size
B	Total bandwidth
S_k	Computational CPU cycles per bit for each task
$\tau_k^{(0)}$	Offloading time for IoT device k
$\tau_k^{(1)}$	Execution time at UAV for IoT device k sub-task
$\tau_k^{(2)}$	Execution time at the remote AP for IoT device k sub-task
$\mathbf{q}$	Horizontal UAV co-ordinates
$\mathbf{h}$	Vertical UAV co-ordinate or height
ϵ	Algorithmic precision

measurements of the propagation channels on a rotary wing UAV. In this regard, the authors derive outage probability as well as root mean square (RMS) delay spread. Then, the authors demonstrated that proper antenna positioning minimizes, whereas high-speed rotating propellers and airframe increase blockage: thus, hampering the communication links. Comparably, the authors in [14] considered dual connectivity in uplink non-orthogonal multiple access (NOMA) for a UAV-assisted terrestrial network. Here, the authors sought to optimize the weighted sum rate through joint optimization of 3D UAV positioning and transmit power allocation. To achieve this objective, the authors proposed a deep deterministic policy gradient algorithm that functions in an offline and an online mode. In this regard, during the offline mode, the algorithm learns a sub-optimal power allocation strategy, whereas in the online mode, it aims to obtain the sub-optimal UAV trajectory policy. In [15], the authors proposed a hybrid physical layer switching policy as well as channel state information (CSI) free UAV selection strategy for analysing the outage probability. In this regard, using their analytical results, the authors showed an end-to-end (E2E) improvement in communication links between BSs and user equipment (UE). Likewise, in [16], the authors studied UAV-assisted vehicular communication system with an aim to maximize the energy efficiency (EE) via optimizing the UAV trajectory. To achieve this goal, the authors transformed the original problem into series of sub-problems and used horizon optimization method. Correspondingly, in [17], the authors examined a novel cooperative jamming strategy for dual UAV-assisted communications to fend off against eavesdroppers. In this regard, the authors suggested a UAV framework, where one UAV transmits useful confidential information to the ground user and the other UAV generates artificial noise to baffle the eavesdropper to secure the transmitted information. Nonetheless, these works [13]–[19], do not consider UAV-enabled MEC systems nor their support for URLLC services.

On one hand, we have a set of works [20]–[24], in technical literature that consider UAV-enabled MEC systems. In [20], the authors studied multi-input single-output (MIS) based UAV-assisted MEC network aiming to minimize the system energy consumption by jointly optimizing CPU frequency, beamforming, transmit power, UAV trajectory and computation tasks. In this regard, the authors also derived the closed-form mathematical expressions for obtaining the optimal transmit power of the UE as well as the CPU frequency at the UAV side. Similarly, in [21], the authors considered multi-UAV-enabled MEC system and sought to optimize resource allocation, power control as well as user association. To achieve this objective, the authors proposed multi-agent reinforcement learning (MARL) as well as multi-agent federated reinforcement learning (MAFRL), which leveraged Gaussian differentials to guarantee privacy for all UE. Comparably, in [22], the authors proposed a UAV-enabled MEC system, where UAV is programmed for data collection from multiple industrial internet-of-things (IoT) devices. Moreover, the authors aimed to mitigate the risk of forest fire by optimizing the maximum response time. To address this issue, the authors proposed a learning-based cooperative particle swarm opti-

mization (LCPSO) for performing resource allocation at the UAV end. Likewise, in [23], the authors studied the problem of maximization of computation-efficiency in UAV-enabled MEC system. In this regard, the authors aimed to maximize the offloaded data as well as minimize the energy consumption at the UAV side. To achieve this goal, the authors performed resource allocation including task scheduling, power control, and bandwidth distribution as well as designed optimal 3D UAV trajectory. Correspondingly, in [24], the authors considered the dual-problems of completion time and energy consumption in the UAV-enabled MEC systems with ground IoT devices. To meet this objective, the authors jointly optimized resource allocation including computation task offloading, energy as well as task constraints and UAV trajectory. It is worth mentioning here that it is a well-known fact that UAVs have limited on-board computational capabilities, thus, a logical conclusion is that it is more optimal to offload a part of the computation task to powerful MEC system present on the ground and execute the remainder of the task at the UAV side. However, these works [20]–[24], do not consider UAV-enabled relaying for MEC systems and only execute the computation tasks at the UAV side which is not ideal.

On the other hand, we have handful of works [25]–[30], that consider facilitating URLLC in UAV-enabled communications. In [25], the authors studied URLLC services for cell free massive multi-input multi-output (MIMO) network where UAVs are supporting the traditional terrestrial network. In this regard, the authors leveraged both partial zero-forcing (PZF) as well as maximum ratio combining (MRC) to perform power control in uplink and downlink communications. Moreover, the authors sought to optimize sum URLLC rate by utilizing successive convex approximations (SCA)-based algorithm. It is worth mentioning that SCA is an iterative optimization technique used to solve non-convex optimization problems. It is particularly effective for problems where the objective function or constraints are non-linear and non-convex. The basic idea behind SCA is to transform a non-convex problem into a series of simpler convex subproblems that can be efficiently solved. Correspondingly, in [26], the authors studied UAV-enabled URLLC services in context of physical layer security. Furthermore, the authors considered air-to-ground (A2G) wireless channel to derive the closed form mathematical expressions for the secrecy outage probability (SOP) as well as the connection outage probability (COP). Likewise, in [27], the authors considered a framework to study URLLC and enhanced mobile broadband (eMBB) services for UAV-enabled relaying system in a terrestrial network. To achieve this objective, the authors formulated a joint multiplexing optimization problem subject to the constraints of bandwidth and transmit power allocation as well as user association with an aim to boost network capacity and minimize transmission power. It is noteworthy that power allocation is a well-known technique for enhancing physical layer security. By optimizing the UAV transmit power contributes to physical layer security by mitigating the risk of information leakage and enhancing the confidentiality of the transmitted data. As such, power allocation results in differences in signal strength, which makes it harder for eavesdroppers to reliably detect and capture all the data packets. In this case, eavesdroppers need to adapt their receivers to handle wide range of power levels, potentially requiring more advanced and flexible receiver systems [31], [32]. As evidenced by previous discussion, UAVs are integral to enabling both URLLC services as well as MEC systems due to their portability and flexible deployment. As such, UAV-enabled MEC systems with URLLC capabilities are crucial because they find their applications in disaster management, industrial automation, healthcare support, public safety, and precision agriculture. These applications involve real-time communication for emergency responders, ultra-responsive control, remote healthcare services, enhanced security, and optimized farming practices [33]–[36]. Nevertheless, these works [25]–[30], do not integrate MEC systems in the framework to facilitate URLLC in UAV-enabled communications, which tends to provide limited insights.

C. Contributions

Despite the vast majority of technical literature relating to UAV-assisted terrestrial networks, an optimization based framework accounting for facilitating URLLC vis-à-vis UAV-enabled relaying for MEC systems in 6G networks is not present. Thus, the novelty as well as the main contributions of this paper are outlined as follows

- We formulate the minimization problem of mission completion time for the joint UAV-enabled relaying and MEC systems in uplink transmissions under short blocklength regime.
- We aim to optimize the resource allocation including the UAV transmit power, UAV CPU frequency, communication bandwidth, blocklength, task partitioning, decoding error rate as well as the 3D UAV positioning.
- We propose three different algorithms including SCA, altered genetic algorithm (AGA), and smart exhaustive search (SES). Afterwards, we selected AGA as the algorithm of our choice thanks to its low-complexity, convergence as well as execution time, which also yields superior performance than other fixed benchmark sub-methods.
- Finally, we show power allocation at the UAV side for different computation tasks to mitigate information leakage and eavesdropping as well as we also demonstrate that 3D UAV positioning is essential for minimization of the decoding error rate to facilitate URLLC services.

D. Organization

We organized the rest of the paper as follows. In Section II, we show the system model and problem formulation. Thereafter, in Section III, we break the original problem into three sub-problems and discuss the SCA-based method. In Section IV, we propose three different algorithms to tackle the original problem. Then, in Section V, we present the simulation results and discussions. Lastly, in Section VI, we conclude the paper and Table I, contains the symbols and their respective descriptions used throughout this paper.

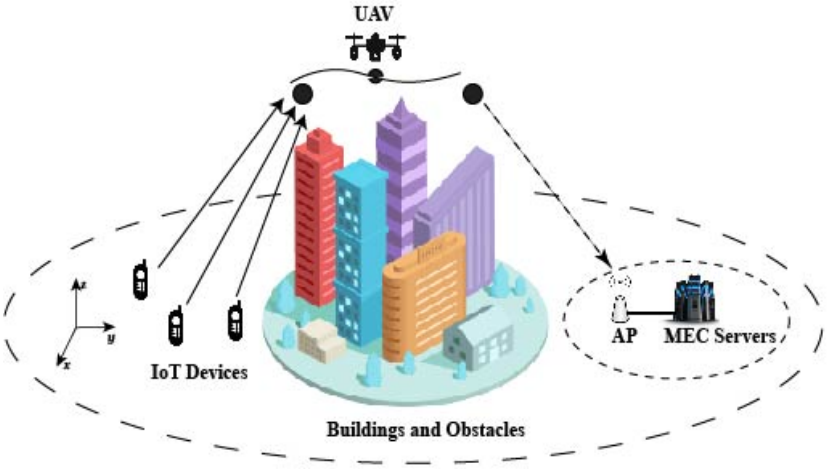

Fig. 1: Illustration of UAV-enabled relaying and MEC systems for URLLC.

II. System Model and Problem Formulation

During uplink transmissions, we simultaneously consider the UAV-enabled relaying and MEC systems, where a rotary-wing UAV[1] is launched to support the execution of the crucial URLLC computation tasks of multiple ground IoT devices, which needs to be transmitted with ultra-high reliability. Moreover, UAV executes a part of the tasks and has an added functionality to act as an aerial relay device to transmit a segment of received tasks from ground IoT devices to a remote access point (AP) for execution as illustrated in Fig. 1. Furthermore, we consider the UAV, IoT devices, and AP are all placed in the 3D Cartesian coordinate system and the coordinates of each IoT device k is depicted as $\mathbf{w}_k = [x_k, y_k, 0]^T$ (meters), where T is the transposition operation. Moreover, the coordinates of remote AP is represented as $\mathbf{w}_{ap} = [x_{ap}, y_{ap}, 0]^T$ (meters), as well as the 3D UAV coordinates are given by $u = [x_u, y_u, z_u]^T$ (meters). For the sake of simplicity, we can further divide and represent UAV's horizontal coordinates as $\mathbf{q} = [x_u, y_u]^T$ (meters) and UAV's vertical coordinates as $\mathbf{h} = z_u$ (meters), respectively. Additionally, UAV, each IoT device, and AP are equipped with single omni-directional antenna respectively. For the sake of generality, we denote the set of IoT devices by $\mathbf{K} = \{1, 2, ..., K\}$, where each IoT device has a crucial URLLC task denoted as $I_k = \{L_k, S_k, O_k\}$. Here, L_k represents the task size (bits), S_k represents the requisite central processing unit (CPU) computational cycles per bit for each task, and O_k represents the computational results size (bits). It is to be noted that $O_k \ll L_k$, thus, it is negligible and it is ignored. Thereafter, we make the assumption that the UAV relay leverages the co-called time-division-duplex (TDD) technique and due to presence of buildings and obstacles between IoT devices and the remote AP the communication links between them are completely blocked. Consequently, each IoT device k task is bound to undergo three phases of transmission and execution including:

- During the first phase, each IoT device k offloads its computation task to the UAV. Simultaneously, the UAV receives and saves the task in its buffer. Here, $\tau_k^{(0)}$ represents the time to offload the task from each IoT device k to the UAV.
- Meanwhile, during the second phase, which includes execution at the UAV side, the offloaded received task is further partitioned into two sub-tasks in accordance to the partition variable denoted by $\mathbf{a}_k$, where $0 \leq \mathbf{a}_k \leq 1$. In this regard, the first sub-task size is denoted by $\mathbf{a}_k L_k$ is computed at the UAV, whereas the second sub-task size given by $(1 - \mathbf{a}_k)\ L_k$ is relayed to the remote AP. Now, $\tau_k^{(1)}$ denotes the time required at the UAV side for performing computation for each IoT device k sub-task, whereas $\tau_k^{(2)}$ depicts the time required for relaying the sub-task from the UAV side to the remote AP. It is noteworthy that by processing a portion of the tasks at the UAV and distributing the remainder to the ground MEC server via AP, the computation cost at the UAV side is reduced.
- Finally, during the third and final phase, the task execution takes place at the remote AP, where the AP receives the relayed sub-task from the UAV side and finishes its computation. Here, $\tau_k^{(3)}$ depicts the time required for computation at the AP for each IoT device k relayed sub-task.

Moreover, to evade interference, each IoT device k is allocated a bandwidth denoted as b_k using orthogonal division multiple access (OFDMA) scheme for the purpose of task offloading and execution during the mission. Furthermore, for practical

[1]The rotary wing UAV in our system model serves as a dynamic relay and mobile edge computing device, providing hovering capabilities and agile maneuverability. Compared to fixed wing UAVs, the rotary wing UAV's vertical take-off and landing (VTOL) capabilities and precise positioning make it the preferred choice for efficient task offloading and resource optimization in our system.

implementation, we denote the channel existing between IoT device k and the UAV by $\mathbf{h}_k$, which is mathematically represented by

$$h_k = \sqrt{\beta_0 d_k^{-\alpha}} g_k, \tag{1}$$

where $d_k^2 = \mathbf{h}^2 + \|\mathbf{q} - \mathbf{w}_k\|^2$ represents the distance existing between each IoT device k and the UAV, β_0 is the channel power gain at the reference distance 1 m, α denotes the path loss exponent, and g_k depicts the small-scale fading random complex variable, such that $\mathbb{E}[|g_k|^2] = 1$. In this context, the small-scale g_k fading is modeled as Rician fading [37], represented by

$$g_k = \sqrt{\frac{\rho_k}{\rho_k + 1}} g + \sqrt{\frac{1}{\rho_k + 1}} \tilde{g}, \tag{2}$$

where g denotes the LoS channel component with $|g| = 1$, $\tilde{g}$ is a circularly symmetric complex Gaussian variable with a zero-mean unit-variance denoting the random scattered component, and ρ_k represents the Rician factor. Now, the channel existing between the UAV and the remote AP channel model is mathematically represented as

$$\begin{aligned} h_r &= \sqrt{\beta_0 d_r^{-\alpha}} g_r, \\ g_r &= \sqrt{\frac{\rho_{kr}}{\rho_{kr} + 1}} g + \sqrt{\frac{1}{\rho_{kr} + 1}} \tilde{g}, \end{aligned} \tag{3}$$

where $d_r^2 = \mathbf{h}^2 + \|\mathbf{q} - \mathbf{w}_{ap}\|^2$ again denotes the distance between the UAV and remote AP, and g_r is the Rician fading. Similarly, g, $\tilde{g}$, and ρ_{kr} represent the aforesaid Rician fading coefficients for the corresponding channel between the UAV and the ground AP. Now, for short blocklengths [38], the data rate[2] $R_k^{(0)}$ (bits per channel use) from each IoT device k to UAV can be mathematically represented by

$$\begin{aligned} R_k^{(0)} &= b_k \log_2(1 + \gamma_{0k}) - \frac{b_k Q^{-1}(\varepsilon_k)}{\ln 2} \sqrt{\frac{V(\gamma_{0k})}{M_k}}, \\ V(\gamma_{0k}) &= 1 - (1 + \gamma_{0k})^{-2}, \\ \gamma_{0k} &= \frac{P_k |h_k|^2}{b_k N_0}. \end{aligned} \tag{4}$$

where P_k represents the transmit power for task offloading of each IoT device k over sub-channel b_k, N_0 denotes the power spectrum density of noise, $V(\gamma_{0k})$ represents channel dispersion, γ_{0k} denotes the SNR between each IoT device k and the UAV, M_k denotes the blocklength allocated to each channel of IoT device k, and $Q^{-1}(\varepsilon_k)$ represents the inverse Gaussian Q-function of decoding error rate ε_k. Similarly, as before, for short blocklengths, the data rate $R_k^{(2)}$ (bits per channel use) required for sending each sub-task of IoT device k from the UAV side to the remote AP can be mathematically written as

$$\begin{aligned} R_k^{(2)} &= b_k \log_2(1 + \gamma_{2k}) - \frac{b_k Q^{-1}(\varepsilon_k)}{\ln 2} \sqrt{\frac{V(\gamma_{2k})}{M_k}}, \\ V(\gamma_{2k}) &= 1 - (1 + \gamma_{2k})^{-2}, \\ \gamma_{2k} &= \frac{p_k |h_r|^2}{b_k N_0}. \end{aligned} \tag{5}$$

where p_k, $V(\gamma_{2k})$, and γ_{2k} represent transmit power, channel dispersion and SNR between the UAV and the remote AP for sending each IoT device k sub-task from the UAV side. Additionally, the UAV transmit power must be limited such that it does not exceed maximum power denoted by P_{max} (Watts). Therefore, we have a constraint on the UAV trasmit power given as

$$\mathcal{C}_1 = \sum_{k=1}^{K} P_k \leq P_{max}, \tag{6}$$

For the sake of simplicity, using [37], we approximate the substitute terms of $|h_k|^2$ and $|h_r|^2$ to abstain from deriving their so-called cumulative distribution functions (CDFs), which are mathematically challenging. Therefore, we can perform mathematical expansions for both γ_{0k} and γ_{2k} as follows

$$\begin{aligned} \gamma_{0k} &= \frac{\beta_0 P_k v_k}{b_k N_0 (\mathbf{h}^2 + \|\mathbf{q} - \mathbf{w}_k\|^2)^{\alpha/2}}, \\ \gamma_{2k} &= \frac{\beta_0 p_k v_k^{(2)}}{b_k N_0 (\mathbf{h}^2 + \|\mathbf{q} - \mathbf{w}_{ap}\|^2)^{\alpha/2}}. \end{aligned} \tag{7}$$

where v_k and $v_k^{(2)}$ are fading power functions given as

$$\begin{aligned} v_k &= K_1 + \frac{K_2}{1 + e^{-J_1 + J_2 u_k}}, \\ u_k &= \frac{\mathbf{h}}{\sqrt{\mathbf{h}^2 + \|\mathbf{q} - \mathbf{w}_k\|^2}}, \\ v_k^{(2)} &= K_1 + \frac{K_2}{1 + e^{-J_1 + J_2 u_2}}, \\ u_k^{(2)} &= \frac{\mathbf{h}}{\sqrt{\mathbf{h}^2 + \|\mathbf{q} - \mathbf{w}_{ap}\|^2}}. \end{aligned} \tag{8}$$

where u_k and $u_k^{(2)}$ are the corresponding sines of the elevation angles. Moreover, the physical constants K_1, K_2 are real numbers from the interval $[0, 1]$ and $K_1 + K_2 = 1$, while constants J_1, J_2 are arbitrary real numbers. Since, the channel dispersion functions given by $V(\gamma_{0k})$ and $V(\gamma_{2k})$ are dependent on their respective SNRs. Hence, we can also rewrite them as

$$\begin{aligned} V(\gamma_{0k}) &= 1 - \left(1 + \frac{\beta_0 P_k v_k}{b_k N_0 (\mathbf{h}^2 + \|\mathbf{q} - \mathbf{w}_k\|^2)^{\frac{\alpha}{2}}}\right)^{-2}, \\ V(\gamma_{2k}) &= 1 - \left(1 + \frac{\beta_0 p_k v_k^{(2)}}{b_k N_0 (\mathbf{h}^2 + \|\mathbf{q} - \mathbf{w}_{ap}\|^2)^{\frac{\alpha}{2}}}\right)^{-2}. \end{aligned} \tag{9}$$

Furthermore, the computations of new tasks are initiated *iff*, the former tasks are sent and executed at the UAV as well as the remote AP sides. Thus, the UAV is capable of performing parallel computations by distributing the optimal

[2]Shannon's rate from the k^{th} IoT device to the UAV is given by $R_k^{(0)} = b_k \log_2(1 + \gamma_{0k})$. However, for short blocklengths, an additional term is included as a penalty to address the limitations of finite blocklengths for URLLC systems. This modified rate is expressed as $R_k^{(0)} = b_k \log_2(1 + \gamma_{0k}) - \frac{b_k Q^{-1}(\varepsilon_k)}{\ln 2} \sqrt{\frac{V(\gamma_{0k})}{M_k}}$, and it accounts for channel dispersion and the variability of the channel. As the blocklength approaches infinity, this penalty term disappears, simplifying it back to Shannon's rate.

CPU frequency for each IoT device k sub-task. Resultantly, we have the following constraint

$$\mathcal{C}_2 = \sum_{k=0}^{K} f_k \leq F_{max}. \tag{10}$$

where f_k denotes the required CPU frequency for computation at the UAV side for each IoT device k sub-task, and F_{max} represents the maximum value of the CPU frequency at any time [39], [40]. It is to noted that the location of AP is fixed, such that it have multiple powerful MEC servers at its disposal [41]. To guarantee that each task of size L_k is completely offloaded, the offloading time $\tau_k^{(0)}$ must satisfy the following constraint

$$\mathcal{C}_3 = \tau_k^{(0)} R_k^{(0)} \geq L_k, \forall k. \tag{11}$$

Similarly, for $\tau_k^{(1)}$ and $\tau_k^{(2)}$, we have the following constraints

$$\mathcal{C}_4 = \tau_k^{(1)} f_k \geq \mathbf{a}_k L_k S_k, \forall k, \tag{12}$$

$$\mathcal{C}_5 = \tau_k^{(2)} R_k^{(2)} \geq (1-\mathbf{a}_k) L_k, \forall k. \tag{13}$$

Thereafter, we define mission completion time denoted by T as the maximum time required for offloading and executing tasks of all IoT devices k, such that we have

$$T \geq \max_{\forall k} \{\tau_k^{(0)} + \tau_k^{(1)}, \tau_k^{(0)} + \tau_k^{(2)}\} \tag{14}$$

Thus, mission completion time minimization problem $\zeta_0 = \{b_k, p_k, f_k, \mathbf{a}_k, \varepsilon_k, \tau_k^{(0)}, \tau_k^{(1)}, \tau_k^{(2)}, \mathbf{q}, \mathbf{h}\}$, for the UAV-enabled relaying for MEC systems is formulated as

$$\mathbf{P0}: \min_{\zeta_0} \; T, \tag{15a}$$

$$\text{s.t.} \quad \mathcal{C}_1 - \mathcal{C}_5, \tag{15b}$$

$$T \geq \tau_k^{(0)} + \tau_k^{(1)}, \forall k, \tag{15c}$$

$$T \geq \tau_k^{(0)} + \tau_k^{(2)}, \forall k, \tag{15d}$$

$$0 \leq \mathbf{a}_k \leq 1, \forall k, \tag{15e}$$

$$0 \leq b_k \leq B, \forall k, \tag{15f}$$

$$\sum_{k=1}^{K} b_k \leq B, \forall k, \tag{15g}$$

$$\varepsilon_k \leq \varepsilon_{max}, \; M_k \leq M_{max} \; \forall k, \tag{15h}$$

$$H_{min} \leq \mathbf{h} \leq H_{max}. \tag{15i}$$

where B (Hz) represents the total allocated bandwidth, ε_{max} is the maximum decoding error of the ground IoT device, referring to the maximum amount of error that can be tolerated in the data packets before communication is considered unreliable. Finally, the last constraint given by eq. (15i), depicts that altitude of UAV is bound within a certain subspace denoted by $[H_{min}, H_{max}]$.

III. SCA-BASED METHOD

It is to be noted that the problem **P0** is non-convex in nature from the non-convexity of $\mathcal{C}_3$, $\mathcal{C}_4$, and $\mathcal{C}_5$. To deal with the non-convexity issue, we will employ successive convex approximations (SCA). As such, the SCA-based method will break the main problem into three sub-problems. Moreover, these sub-problems denoted by ζ_1, ζ_2, ζ_3 are the optimization of different variables represented as

$$\begin{aligned} \zeta_1 &= \{b_k, p_k, f_k, \mathbf{a}_k, \varepsilon_k, \tau_k^{(0)}, \tau_k^{(1)}, \tau_k^{(2)}\}, \\ \zeta_2 &= \{\varepsilon_k, \tau_k^{(0)}, \tau_k^{(2)}, \mathbf{q}\}, \\ \zeta_3 &= \{\varepsilon_k, \tau_k^{(0)}, \tau_k^{(2)}, \mathbf{h}\}. \end{aligned} \tag{16}$$

It is to be noted that the SCA-based method will solve these three sub-problems in an iterative manner to yield sub-optimal results.

A. Sub-problem of Resource Allocation

We obtain the first sub-problem by fixing q and H, both of which represent the 3D UAV positioning. Therefore, the optimization problem ζ_1 is formulated as

$$\mathbf{P1}: \min_{\zeta_1} T, \tag{17a}$$

$$\text{s.t.} \quad \mathcal{C}_1 - \mathcal{C}_5, \tag{17b}$$

$$(15\text{c}) - (15\text{h}). \tag{17c}$$

Now, the constraint $\mathcal{C}_3$ could be transformed to a convex one by using slack variable $s_k^{(0)} > 0$. Thus, by using first order Taylor series expansion, we have

$$\begin{aligned} (\tau_k^{(0)j} + s_k^{(0)j})^2 + 2(\tau_k^{(0)j} + s_k^{(0)j})(\tau_k^{(0)} + s_k^{(0)} - \\ - \tau_k^{(0)j} - s_k^{(0)j}) - (\tau_k^{(0)} - s_k^{(0)})^2 \geq 4L_k, \end{aligned} \tag{18}$$

$$s_k^{(0)} \leq b_k \log_2(1+\gamma_{0k}) - \frac{b_k Q^{-1}(\varepsilon_k)}{\ln(2)} \sqrt{\frac{V(\gamma_{0k})}{M_k}}, \tag{19}$$

According to [42], the right hand side of eq. (19) is convex and it is a decreasing function w.r.t. γ_{0k}, such that we have

$$\frac{1}{\gamma_{0k}} \leq g^{-1}\left(\frac{Q^{-1}(\varepsilon_k)}{\sqrt{M_k}}\right), \tag{20}$$

Now, by rearranging eq. (20) in terms of x, we have

$$g(x) = \frac{(x+1)\ln(\frac{1}{x}+1)}{\sqrt{2x+1}}. \tag{21}$$

For the sake of mathematical analysis, we assume M_k equal to 200 symbols and a decoding error rate ε_k is less then 10^{-7}. According to the reference values of γ_{0k} function, we can set $Q^{-1}(\varepsilon_k)$ as approximately 4.25. Therefore, we have following criteria for concavity of the eq. (18) and eq. (19) w.r.t. γ, given as

$$\gamma_k \geq \gamma_* = \frac{1}{g^{-1}(\frac{4.25}{\sqrt{200}})} \approx \frac{1}{g^{-1}(0.3)} \approx 1/6.05 \approx 0.16 \tag{22}$$

However, this criteria is not sufficient for our problem. Therefore, in order to calculate and estimate convexity criteria more precisely, we approximate the values of $Q^{-1}(\varepsilon_k)$ and $V(\gamma_{0k})$, and we rewrite eq. (19) as

$$\begin{aligned} s_k^{(0)} &\leq b_k \log_2(1+\gamma_{0k}) - b_k \eta \sqrt{1-(1+\gamma_{0k})^{-2}}, \\ \eta &= \frac{Q^{-1}(\varepsilon_k)}{\ln(2)\sqrt{M}} \approx \frac{4.25}{\ln 2\sqrt{200}} \approx 0.43. \end{aligned} \tag{23}$$

where η is a constant value as shown above. Thus, for the sake of simplicity, we rewrite eq. (23), and its first and second derivatives w.r.t. x as

$$\begin{aligned} y(x) &= \log_2(1+x) - \eta\sqrt{1-(1+x)^{-2}}, \\ y'(x) &= \frac{1}{(x+1)\ln(2)} - \frac{\eta}{\sqrt{1-(x+1)^{-2}}(x+1)^3}, \\ y''(x) &= \frac{3\eta}{\sqrt{1-(x+1)^{-2}}(x+1)^4} - \frac{1}{(x+1)^2\ln 2} \\ &\quad + \frac{\eta}{(1-(x+1)^{-2})^{3/2}(x+1)^6}. \end{aligned} \tag{24}$$

Here, the mathematical analysis of this function shows us that for the value of $x < \lambda_*$, function $y''(x) > 0$ for the values $x > \lambda_*$ function $y''(x) < 0$. In this regard, with the help of binary search, we can find the value of the $\lambda_* \approx 0.38$. Moreover, it is to be noted that the values of transmission rates $R_k^{(0)} > 0$ and $R_k^{(2)} > 0$, otherwise inequalities eq. (11) and eq. (13) cannot be satisfied. In this regard, the analysis of eq. (24) and its derivative shows that it has one root equal to zero, and no more than one positive root. For the value $\eta = 0.43$, this root, is found by either utilizing binary search or Newton method which comes out to be $\lambda_0 \approx 0.164 < \lambda_*$. Thus, by eliminating boundary conditions, we have the necessary condition given by

$$\gamma_{2k} = \frac{\beta_0 p_k v_k^j}{b_k N_0 (\mathbf{h}^j)^2 + \|\mathbf{q}^j - \mathbf{w}_k\|^2)^{\alpha/2}} \geq \lambda_*. \tag{25}$$

Now, constraint $\mathcal{C}_4$ can be transformed as

$$\begin{aligned} (\tau_k^{(1)j} + f_k^j)^{(2)} + 2(\tau_k^{(1)j} + f_k^j)(\tau_k^{(1)} + f_k - \tau_k^{(1)j} - f_k^j) \\ - (\tau_k^{(1)} - f_k)^2 \geq 4\mathbf{a}_k L_k S_k. \end{aligned} \tag{26}$$

Similarly, constraint $\mathcal{C}_5$ can be transformed as

$$\begin{aligned} (\tau_k^{(2)j} + s_k^{(2)j})^2 + 2(\tau_k^{(2)j} + s_k^{(2)j})(\tau_k^{(2)} + s_k^{(2)} - \tau_k^{(2)j} - s_k^{(2)j}) \\ - (\tau_k^{(2)} - s_k^{(2)})^2 \geq 4(\mathbf{a}_k) L_k. \end{aligned} \tag{27}$$

Thereafter, the condition for slack variable will be

$$s_k^{(2)} \leq b_k \log_2(1+\gamma_{2k}) - b_k\eta\sqrt{1-(1+\gamma_{2k})^{-2}}, \tag{28}$$

Again, we can approximate eq. (28) by

$$\begin{aligned} s_k^{(2)} &\leq b_k \log_2\left(1 + \frac{\beta_0 p_k v_k^j}{b_k N_0((\mathbf{h}^j)^2 + \|\mathbf{q}^j - \mathbf{w}_{ap}\|^2)^{\alpha/2}}\right) \\ &- b_k\eta\sqrt{1 - \left(1 + \frac{\beta_0 p_k v_k^j}{b_k N_0((\mathbf{h}^j)^2 + \|\mathbf{q}^j - \mathbf{w}_{ap}\|^2}\right)^{-2}}. \end{aligned} \tag{29}$$

Hence, **P1** optimization problem can be reformulated as

$$\begin{aligned} \mathbf{P1.1}: \min_{\zeta_1} \; & T, \\ \text{s.t.} \quad & \mathcal{C}_1, \mathcal{C}_2, \\ & (15\text{h}), (18), (19), \\ & (26) - (29), \\ & \gamma_{2k} \geq \lambda_*, \forall k. \end{aligned}$$

It is to be noted that **P1.1** is a convex optimization problem, which can leverage convex optimization tools, i.e., CVX.

B. Sub-problem of Horizontal UAV Positioning

We formulate the second sub-problem of UAV positioning[3] by fixing $\{b_k, p_k, f_k, \mathbf{a}_k, \tau_k^{(1)}, \mathbf{h}\}$. Thus, we can rewrite ζ_2 as

$$\mathbf{P2}: \min_{\zeta_2} T, \tag{30a}$$

$$\text{s.t.} \quad \mathcal{C}_3, \mathcal{C}_5, \tag{30b}$$

$$(15\text{c}), (15\text{d}), (15\text{h}). \tag{30c}$$

As evidenced before, the constraints $\mathcal{C}_3$ and $\mathcal{C}_5$ are non-convex in nature. To remedy this issue, we use the same approach as in previous sub-problem and we create slack variables denoted by $s_k^{(0)}$ and $s_k^{(2)}$. Therefore, we have

$$\begin{aligned} s_k^{(0)} &\leq b_k^j \log_2\left(1 + \frac{\beta_0 P_k v_k}{b_k^j N_0((\mathbf{h}^j)^2 + \|\mathbf{q} - \mathbf{w}_k\|^2)^{\frac{\alpha}{2}}}\right) \\ &- b_k^j \eta\sqrt{1 - \left(1 + \frac{\beta_0 P_k v_k}{b_k^j N_0((\mathbf{h}^j)^2 + \|\mathbf{q} - \mathbf{w}_k\|^2)^{\frac{\alpha}{2}}}\right)^{-2}}, \end{aligned} \tag{31}$$

$$\begin{aligned} s_k^{(2)} &\leq b_k^j \log_2\left(1 + \frac{\beta_0 p_k^j v_k}{b_k^j N_0((\mathbf{h}^j)^2 + \|\mathbf{q}^j - \mathbf{w}_{ap}\|^2)^{\frac{\alpha}{2}}}\right) \\ &- b_k^j \eta\sqrt{1 - \left(1 + \frac{\beta_0 p_k^j v_k}{b_k^j N_0((\mathbf{h}^j)^2 + \|\mathbf{q} - \mathbf{w}_{ap}\|^2)^{\frac{\alpha}{2}}}\right)^{-2}}. \end{aligned} \tag{32}$$

Now, the given **P2** can be transformed to the convex problem by further transforming eq. (32) and using constants $A_{k1} = \frac{\beta_0 p_k K_1}{b_k^j N_0}$, $A_{k2} = \frac{\beta_0 P_k K_2}{b_k^j N_0}$ and introducing t_k, x_k, y_k, z_k as new slack variables. Thereafter, we have

$$s_k^{(0)} \leq b_k^j \log_2(1+t_k) - b_k^j \eta\sqrt{1-(1+t_k)^2}, \tag{33a}$$

$$t_k \geq \lambda_*, \tag{33b}$$

$$t_k \leq \frac{A_{k1} + \frac{A_{k2}}{x_k}}{y_k^{\alpha/2}}, \tag{33c}$$

$$x_k \leq 1 + e^{-z_k}, \tag{33d}$$

$$y_k \leq \|\mathbf{q} - \mathbf{w}_k\|^2 + (\mathbf{h}^j)^2, \tag{33e}$$

$$z_k \leq J_1 + J_2 u_k. \tag{33f}$$

Similarly, we deal with the non-convexity of eq. (33c) and eq. (33f). It is to be noted that the right hand side of eq. (33c) is convex w.r.t. x_k and y_k (please refer to Appendix A). Thus, for any given x_k and y_k, the right hand side of eq. (33c) is converted to a lower bound function denoted

[3]The considered UAV-assisted communication system does not utilize a snake traversal trajectory but focuses on optimizing 3D UAV positioning. As such, mapping a snake traversal trajectory is unsuitable for the system as it leads to inefficient resource allocation and communication performance. Moreover, the system's objectives of task offloading and mobile edge computing require a more structured and predictable UAV positioning approach for optimal performance and reliable communications.

by $\phi_k^{lb}(A_{k1}, A_{k2}, x_k, y_k)$. Therefore, by SCA method, we can write

$$\begin{aligned} t_k &\le \phi_k^{lb}(A_{k1}, A_{k2}, x_k, y_k), \\ \phi_k^{lb}(A_{k1}, A_{k2}, x_k, y_k) &= \frac{A_{k1} + A_{k2}(x_k^j)^{-1}}{(y_k^j)^{\alpha/2}} - \frac{A_{k2}(x_k - x_k^j)}{(x_k^j)^{(2)}(y_k^j)^{\alpha/2}} \\ &\quad - \frac{\alpha(A_{k1} + A_{k2}(x_k^j)^{-1})}{2(y_k^j)^{\alpha/2+1}}(y_k - y_k^j). \end{aligned} \tag{34}$$

Likewise, to tackle the non-convexity of eq. (33f), since u_k is convex w.r.t. $(\mathbf{h}^j)^2 + \|\mathbf{q}^j - \mathbf{w}_k\|^2$ (please refer to Appendix B), we obtain lower the bound of u_k denoted by $\psi_k^{lb}(\mathbf{w}_k, \mathbf{q})$, which can be mathematically represented as

$$\begin{aligned} \psi_k^{lb}(\mathbf{w}_k, \mathbf{q}) &= \frac{\mathbf{h}^j}{\sqrt{(\mathbf{h}^j)^2 + \|\mathbf{q}^j - \mathbf{w}_k\|^2}} \\ &\quad - \frac{\mathbf{h}^j(\|\mathbf{q} - \mathbf{w}_k\|^2 - \|\mathbf{q}^j - \mathbf{w}_k\|^2)}{2((\mathbf{h}^j)^2 + \|\mathbf{q}^j - \mathbf{w}_k\|^2)^{3/2}}, \\ z_k &\le J_1 + J_2\psi_k^{lb}(\mathbf{w}_k, \mathbf{q}). \end{aligned} \tag{35}$$

Therefore, for $s_k^{(2)}$, the constraints given above converted into

$$s_k^{(2)} \le B_k^j \log_2(1 + \hat{t_k}) - B_k^j \eta V(\bar{t_k}), \tag{36a}$$
$$\bar{t_k} \ge \lambda_*, \tag{36b}$$
$$\bar{t_k} \le \psi_k^{lb}(\bar{A_{k1}}, \bar{A_{k2}}, \bar{x}, \bar{y}), \tag{36c}$$
$$\bar{x} \le 1 + e^{-\bar{z}}, \tag{36d}$$
$$\bar{y} \le \|\mathbf{q} - \mathbf{w}_k\|^{(2)} + (\mathbf{h}^j)^2, \tag{36e}$$
$$\bar{z} \le J_1 + J_2\psi_k^{lb}(\mathbf{w}_{ap}, \mathbf{q}). \tag{36f}$$

where $\bar{A_{k1}} = \frac{\beta_0 p_{kr}^j K_1}{b_k^j N_0}$, and $\bar{A_{k2}} = \frac{\beta_0 p_k^j K_2}{b_k^j N_0}$. Resultantly, **P2** aiming to optimize $\zeta_{2.1} = \{\tau_k^{(0)}, \tau_k^{(2)}, \mathbf{q}, s_k^{(0)}, t_k, x_k, y_k, z_k, s_k^{(2)}, \bar{t_k}, \bar{x}, \bar{y}, \bar{z}\}$ can be reformulated as

$$\begin{aligned} \mathbf{P2.1}: &\min_{\zeta_{2.1}} T, \\ \text{s.t.} \quad &(15\text{c}), (15\text{d}), (15\text{h}), \\ &(19), (27), (34\text{a}), \\ &(34\text{b}), (34\text{d}), (34\text{e}), \\ &(35), (36), (37). \end{aligned}$$

Now, **P2.1** is reduced to a convex problem and the sub-problem of horizontal UAV positioning can be efficiently tackled.

C. Sub-problem of Vertical UAV Positioning

Finally, we formulate the third sub-problem by fixing $\{b_k, p_k, f_k, \mathbf{a}_k, \tau_k^{(1)}, \mathbf{q}\}$. Therefore, ζ_3 can be formulated as

$$\mathbf{P3}: \min_{\zeta_3} T, \tag{37a}$$
$$\text{s.t.} \quad \mathcal{C}_3, \mathcal{C}_5, \tag{37b}$$
$$(15\text{c}), (15\text{d}), (15\text{h}), (15\text{i}). \tag{37c}$$

Here, we leverage the SCA method, since u_k and u_k^2 are convex w.r.t. $\mathbf{h}$ (please refer to Appendix C), we compute the lower bound functions, which are represented by ϕ_k^{lb} and χ^{lb}, given as

$$\begin{aligned} \phi_k^{lb}(\mathbf{w}_k, \mathbf{q}) =& \frac{\mathbf{h}^j}{\sqrt{(\mathbf{h}^j)^2 + \|\mathbf{q}^j - \mathbf{w}_k\|^2}} + \frac{\mathbf{h} - \mathbf{h}^j}{\sqrt{\|\mathbf{q}^j - \mathbf{w}_k\|^2 + (\mathbf{h}^j)^2}} \\ &- \frac{(\mathbf{h} - \mathbf{h}^j)(\mathbf{h}^j)^2}{(\|\mathbf{q}^j - \mathbf{w}_k\|^2 + (\mathbf{h}^j)^2)^{3/2}}, \end{aligned} \tag{38}$$

$$\chi^{lb} = \phi_k^{lb}(\mathbf{w}_{ap}, \mathbf{h}). \tag{39}$$

Consequently, **P3** seeking to optimize $\zeta_{3.1} = \{\tau_k^{(0)}, \tau_k^{(2)}, \mathbf{h}, s_k^{(0)}, t_k, x_k, y_k, z_k, s_k^{(2)}, \bar{t_k}, \bar{x}, \bar{y}, \bar{z}\}$ can be reformulated as

$$\begin{aligned} \mathbf{P3.1}: &\min_{\zeta_{3.1}} T, \\ \text{s.t.} \quad &\mathcal{C}_3, \mathcal{C}_5, (15\text{c}), \\ &(15\text{d}), (15\text{h}), \\ &(16), (27), \\ &(33\text{a}) - (33\text{f}), \\ &(36\text{a}) - (36\text{f}), \\ &z_k \le J_1 + J_2\phi_k^{lb}, \\ &\hat{z} \le J_1 + J_2\chi^{lb}. \end{aligned}$$

Therefore, the problem **P3.1** is convex, which can be solved by convex optimization solvers as mentioned before.

IV. Proposed Algorithms

A. SCA-based Algorithm

Due to the analysis shown before, we present an effective algorithm, namely **Algorithm 1**, where we employ the SCA-based method to divide our main problem **P0** into three smaller sub-problems namely **P1.1**, **P2.1**, and **P3.1**. As discussed before, the main problem **P0** is non-convex, hence, a global solution is not guaranteed. Nonetheless, we know that objective function in each sub-problem is not increasing and it has lower bounds. Therefore, we can perform local optimization for each of the sub-problems, and the **Algorithm 1** is at least guaranteed to converge to a locally optimal solution. Firstly, the algorithm begins by initializing various input parameters such as K, L_k, S_k for all k, F_{max}, B, P_{max}, H_{min}, H_{max}, N_0, β_0, α, K_1, K_2, J_1, and J_2. Additionally, it sets initial values for variables including $j = 0$, $\varepsilon_{max} = 10^{-7}$, and $M_{max} = 200$ symbols. The core idea of the algorithm is to iteratively solve three sub-problems, denoted as **P1.1**, **P2.1**, and **P3.1**, within a while loop. In each iteration, the algorithm updates the values of various parameters and variables based on the solutions obtained from the previous iteration. As such, the algorithm aims to minimize the absolute difference between two consecutive values of T^j until it falls below a predefined precision value ϵ. The first sub-problem, **P1.1**, is solved by providing the initial values of $\mathbf{q}^j$ and $\mathbf{h}^j$, which yields optimal solutions for variables such as b_k^j, f_k^j, $\mathbf{a}_k^j$, $\tau_k^{(0)j}$, $\tau_k^{(1)j}$, and $\tau_k^{(2)j}$. Then, using these results, the algorithm proceeds to solve **P2.1**, where it calculates the optimal solutions for $\tau_k^{(0)j}$, $\tau_k^{(2)j}$, and $\mathbf{q}^j$, while keeping b_k^j, f_k^j, $\mathbf{a}_k$, $\tau_k^{(1)j}$, and $\mathbf{h}^{j+1}$ fixed. Finally, **P3.1** is solved using updated values of b_k^j, f_k^j, $\mathbf{a}_k^j$,

$\tau_k^{(1)j}$, and $\mathbf{q}^{j+1}$ to find the optimal solutions denoted by $\tau_k^{(0)j}$, $\tau_k^{(2)j}$, and $\mathbf{h}^j$. Lastly, this process repeats by incrementing the value of j until the convergence condition $|T^j - T^{j-1}| \leq \epsilon$ is met.

Algorithm 1: SCA-based Algorithm for solving problem **P0**

Input K, L_k, S_k, p_k, $\forall k$, F_{max}, B, P_{max}, H_{min}, H_{max}, N_0, β_0, α, K_1, K_2, J_1, J_2,
Set $j = 0$, $\varepsilon_{max} = 10^{-7}$ and $M_{max} = 200$ symbols,
Initialize $\{\mathbf{q}^{(0)},\ \mathbf{h}^{(0)}\}$, and a precision ϵ,
while $|T^j - T^{j-1}| \leq \epsilon$ **do**
  Solve **P1.1** with given $\{\mathbf{q}^j,\ \mathbf{h}^j\}$ and obtain the optimal solutions of $\{b_k^j, p_k^j, f_k^j, \mathbf{a}_k^j, \tau_k^{(0)j}, \tau_k^{(1)j}, \tau_k^{(2)j}\}$
  Solve **P2.1** with given $\{b_k^j, p_k^j, f_k^j, \mathbf{a}_k, \tau_k^{(1)j}, \mathbf{h}^{j+1}\}$ and obtain the optimal solutions of $\{\tau_k^{(0)j}, \tau_k^{(2)j}, \mathbf{q}^j\}$
  Solve **P3.1** with given $\{b_k^j, p_k^j, f_k^j, \mathbf{a}_k^j, \tau_k^{(1)j}, \mathbf{q}^{j+1}\}$ and obtain the optimal solutions denoted by $\{\tau_k^{(0)j}, \tau_k^{(2)j}, \mathbf{h}^j\}$
  Set $j = j + 1$.
end
Return an optimized solution

B. Altered Genetic Algorithm

Now, we briefly describe all the steps of Altered Genetic Algorithm (AGA), which uses SCA as a means for improvement in **Algorithm 2**. The main idea behind the AGA-based Algorithm involves a series of steps that combine genetic algorithm principles with SCA inequalities. As such, the algorithm starts by receiving input parameters such as K, L_k, S_k for all k, F_{max}, B, P_{max}, H_{min}, H_{max}, N_0, β_0, α, K_1, K_2, J_1, and J_2. It initializes variables including j, ε_{max}, M_{max}, and $\mathcal{X}$, an array initialized with zeros that will store the optimized solutions. Within a while loop, the algorithm aims to minimize the absolute difference between two consecutive values of T^j until it falls below a predefined threshold ϵ or until the maximum number of iterations $\mathcal{G}$ is reached. Each iteration involves several crucial steps, including probabilities calculation, crossover, mutation, and selection. During the probabilities calculation step, the algorithm calculates the sum of values Φ^j and determines the probabilities of selection Φ_i^j for each value. Thereafter, in the crossover step, pairs for crossover are selected based on their probabilities, and new points $\mathcal{P}_1''$ and $\mathcal{P}_2''$ are obtained using random number generators and mathematical formulas. Then, the mutation step introduces random changes to the coordinates of selected points. Subsequently, the selection step populates the array $\mathcal{X}$ with the obtained points and their corresponding values, removing the points with the smallest values and retaining only the m points with the lowest values. Additionally, the algorithm evaluates an iteration criteria to determine whether to continue or terminate the iteration process. If the maximum value from $\mathcal{X}$ remains unchanged and the distance between the two most optimal solutions is less than ϵ, the algorithm increments j by 1; otherwise, it resets j to 0. Overall, the inclusion of SCA inequalities adds an additional optimization aspect to the AGA-based algorithm, allowing it to find solutions that satisfy these inequalities to improve the performance. Lastly, the algorithm terminates based on convergence criteria and returns the optimized solution found during the iterations.

Algorithm 2: AGA-based Algorithm for solving **P0**

Input K, L_k, S_k $\forall k$, F_{max}, B, P_{max}, H_{min}, H_{max}, N_0, β_0, α, K_1, K_2, J_1, J_2.
Set $j = 0$, $\varepsilon_{max} = 10^{-7}$, $M_{max} = 200$ symbols, and $\mathcal{X}$ of $\mathcal{M}$ denoted by $(b_k, p_k, f_k, \mathbf{a}_k, \tau_k^{(0)}, \tau_k^{(1)}, \tau_k^{(2)}, \mathbf{q}, \mathbf{h})$ values to zeros.
Initialize Random m values denoted by $\mathcal{P}_i^j$, inside the given domain, and the maximum number of iterations without progress in finding the solution $\mathcal{G}$. For all the other points, the maximum value denoted by θ_i, such that point $\hat{\mathcal{P}}_i^j = \mathcal{P}^j + \theta_i e_i$, where $e_i \in (-1, 1)$, for the SCA inequalities in **P1.1**, **P2.1**, and **P3.1**, is found using Newton method and corresponding maximum values of T_i^j is stored.
while $|T^j - T^{j-1}| \leq \epsilon,\ j < \mathcal{G}$ **do**
  Probabilities calculation The sum of values given by $\Phi^j = \sum_{i=0}^{m} T_i^j$ is calculated and probabilities of selection $\Phi_i^j = T_i^j / \Phi^j$ for each values are obtained
  Crossover The pairs for crossover w.r.t. their probabilities Φ_i^j are selected. For each such pair (P_1', P_2'), where $\mathcal{P}_1'$ is selected in such a way, that its value of T_i^j is greater then those of $\mathcal{P}_2'$, the points $\mathcal{P}_1''$ and $\mathcal{P}_2''$ are obtained by formulae $\mathcal{P}_1'' = \Phi((\mathcal{P}_1' + \mathcal{P}_2')/2))$ and $\mathcal{P}_2'' = \Phi(\mathcal{P}_1' - \mathcal{P}_2'/2))$, where $\Phi(x)$ is random number generator with normal distribution and mean x. Thereafter, we select random point $\mathcal{P}_0$, and for points $\mathcal{P}_1''$ and $\mathcal{P}_2''$ the maximum values of θ_1'' and θ_2'' are calculated, such that $\hat{\mathcal{P}}_i'' = \mathcal{P}_i'' \theta_i''$, satisfies the SCA inequalities in **P1.1**, **P2.1**, and **P3.1**.
  Mutation With fixed small probability φ, one of the coordinates of point $\mathcal{P}_i''$ is changed randomly and corresponding value of $\hat{\mathcal{P}}_i''$ is obtained.
  Selection Place values of $\hat{\mathcal{P}''}_i^j$ with their corresponding values of T_i^j into $\mathcal{X}$. Thereafter, remove the values of $\mathcal{X}$ that correspond to the smallest values of T, in order to leave the m values with the lowest T values
  Iteration criteria If maximum value from $\mathcal{X}$ was not changed, and the distance between two most optimal solutions is less then ϵ, then set $j = j + 1$, else set $j = 0$
end
return an optimized solution

C. Smart Exhaustive Search-based Algorithm

Algorithm 3: SES-based Algorithm for solving **P0**

Input K, L_k, S_k, P_k, $\forall k$, F_{max}, B, P_{max}, H_{min}, H_{max}, N_0, β_0, α, K_1, K_2, J_1, J_2,
Set $j = 0$, $\varepsilon_{max} = 10^{-7}$, $M_{max} = 200$ symbols, set vector $\mathcal{X}$ of $\mathcal{M}$ denoted by $(b_k, p_k, f_k, \mathbf{a}_k, \tau_k^{(0)}, \tau_k^{(1)}, \tau_k^{(2)}, \mathbf{q}, \mathbf{h})$ equal to zeros,
Initialize The number of generated vectors m, the maximum number of iterations without progress in finding the solution $\mathcal{G}$, the number of stored optimums $\mathcal{M}$, and precision ϵ,
while $|T^j - T^{j-1}| \leq \epsilon$, $|T_1^j - T_0^j| \leq \epsilon$, $j < \mathcal{G}$ **do**
  Generate random point $\mathcal{P}^j$ in $\mathcal{Q}$
  If $\mathcal{P}^j$ does not satisfy inequalities in **P0**, then repeat previous step
  Generate random vectors $e_1, e_2, \ldots, e_m$
  Using binary search find maximum value of θ_i, if that point $\hat{\mathcal{P}}_i^j = \mathcal{P}^j + \theta_i e_i$, where $e_i \in (-1, 1)$, satisfies inequalities in **P0**, then store corresponding maximums to vector T_i^j
  Put values of $\hat{\mathcal{P}}_i^j$ and of T_i^j into $\mathcal{X}$
  Remove from $\mathcal{X}$, those values corresponding to the smallest m values of T_i^j
  If maximum value from $\mathcal{X}$ was not changed, then set $j = j + 1$, else set $j = 0$
end
return an optimized solution

Smart exhaustive search algorithm (SES) uses the random walk strategy. In this regard, we select some random point $\mathcal{P}$ in the subspace of the variables b_k, p_{rk}, f_{rk}, $\mathbf{a}_k$, $\tau_k^{(0)}$, $\tau_k^{(1)}$, $\tau_k^{(2)}$, $\mathbf{q}$, $\mathbf{h}$ within our domain. In this regard, if this point does not satisfy our inequalities in **P0**, then we do not consider it and then generate another one. Otherwise, we can select random vector(s), i.e., $e_1, e_2, \ldots, e_m$ in our space denoted by $\mathcal{Q}$. Thereafter, we find maximum values of T for each line, that is built from $\mathcal{P}$ in the directions of $e_1, e_2, \ldots, e_m$. Furthermore, we repeat this process until the overall found maximum value of T stops decreasing for a large number of iterations denoted by $\mathcal{D}$. It is to be noted that some $\mathcal{M}$ optimal values are stored as vectors of coordinates $x_1, x_2, \ldots, x_{\mathcal{M}}$. Hereafter, each time we select $e_1, e_2, \ldots, e_m$ representing random vectors for the directions from $\mathcal{P}$, where $e_i \in (-1, 1)$, we select them in such a way that they are close with some probability to the coordinates $x_1, x_2, \ldots, x_{\mathcal{M}}$. Then, we update values of found maximum values $x_1, x_2, \ldots, x_{\mathcal{M}}$. Finally, we can summarize all the steps of so-called SES in **Algorithm 3**.

D. Time-Complexity of Proposed Algorithms

In this sub-section, we estimate the effectiveness of the previously described proposed algorithms in finding the optimums in terms of maximum amounts of operations they require to obtain the given results with given precision $\epsilon > 0$. Firstly, we note that the effectiveness of the SCA-based approach is difficult to calculate because of the unclear speed of convergence to the local optimum at each stage step of the **Algorithm 1** for every sub-problem **P1.1**, **P2.1**, and **P3.1**. Nonetheless, we can consider estimation given in [43], which postulates that convex optimization algorithm converges sub-linearly to the local solution. Thus, total time of the sub-problems **P1.1**, **P2.1**, and **P3.1** is denoted by $\mathcal{O}(-\ln(\epsilon)^2)$. Furthermore, we also consider speed of convergence of the **Algorithm 1**. In this regard, the present research such as [44], do not provide sufficient theory on the speed of convergence for SCA algorithms. However, we know from the the nature of the method that the convergence speed is linearly dependant on the number of space dimensions of the given variables, whose time-complexity is given as $\mathcal{O}(-\ln(\epsilon)^4)$. Therefore, total complexity of the **Algorithm 1** after simplification is denoted by is $\mathcal{O}(-N\ln(\epsilon))$ or $\mathcal{O}(N\ln(1/\epsilon))$, where N represents the number of iterations. Now, it is to be noted that for the AGA, the complexity of our **Algorithm 2** is $\mathcal{O}(N\mathcal{S}\mathcal{K})$, where N represents the number of iterations and $\mathcal{S}$ denotes the population size, and $\mathcal{K}$ depicts the problem variables. Thereafter, for SES, the time-complexity is given by $\mathcal{O}\left(\mathcal{A}\mathcal{B}^2 \times \mathcal{P} \times \mathcal{F} \times \mathcal{T}^3 \times \mathcal{Q}\mathcal{H}^2\right)$, where the number of points tested for both a_k and b_k is represented by $\mathcal{A}\mathcal{B}$, for p_k is denoted by $\mathcal{P}$, for f_k is depicted as $\mathcal{F}$, and for each of $\mathbf{q}$ and $\mathbf{h}$ is $\mathcal{Q}\mathcal{H}$. It is to be noted that we choose $\mathcal{A}\mathcal{B} = \mathcal{P} = \mathcal{F} = \mathcal{T} = \mathcal{Q}\mathcal{H} = 10000$ points, which makes the SES complexity much greater than that of the proposed **Algorithm 1** and **Algorithm 2**. Finally, we deduce that AGA can efficiently solve **P0**, by the virtue of having lowest complexity.

V. Simulation Results and Discussions

In this section, we set various systems parameters in Table II. It is to be noticed that the selection of constant parameter values for our deterministic optimization problem involved a combination of theoretical knowledge, problem characteristics, sensitivity analysis, and iterative refinement. By leveraging existing knowledge, understanding problem properties, evaluating parameter sensitivity, and iteratively refining values based on hit and trial method, we achieved optimized parameter configurations.

TABLE II: System Parameters

Parameters	Numerical values
$\varepsilon_{\max}$	10^{-7}
$M_{\max}$	200 symbols
ϵ	10^{-5}
B	10 MHz
$P_{\max}$	30 dBmW
K	8 IoT devices
$F_{\max}$	5 GHz
S_k	10^3 cycles/bit
L_k	30 Mb
β_0	-60 dB
N_0	-169 dBm
K_1	-4.7
K_2	8.9
J_1	0.01
J_2	0.99
α	2.3
$H_{\min}$	80 m
$H_{\max}$	200 m

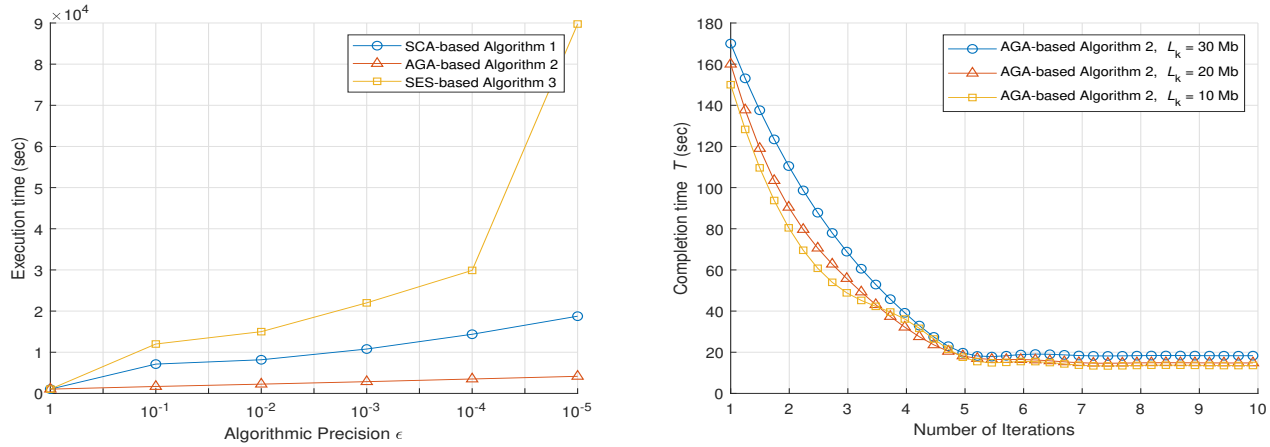

(a) (b)

Fig. 2: (a) Execution time versus Algorithmic precision (b) Completion time versus number of iterations.

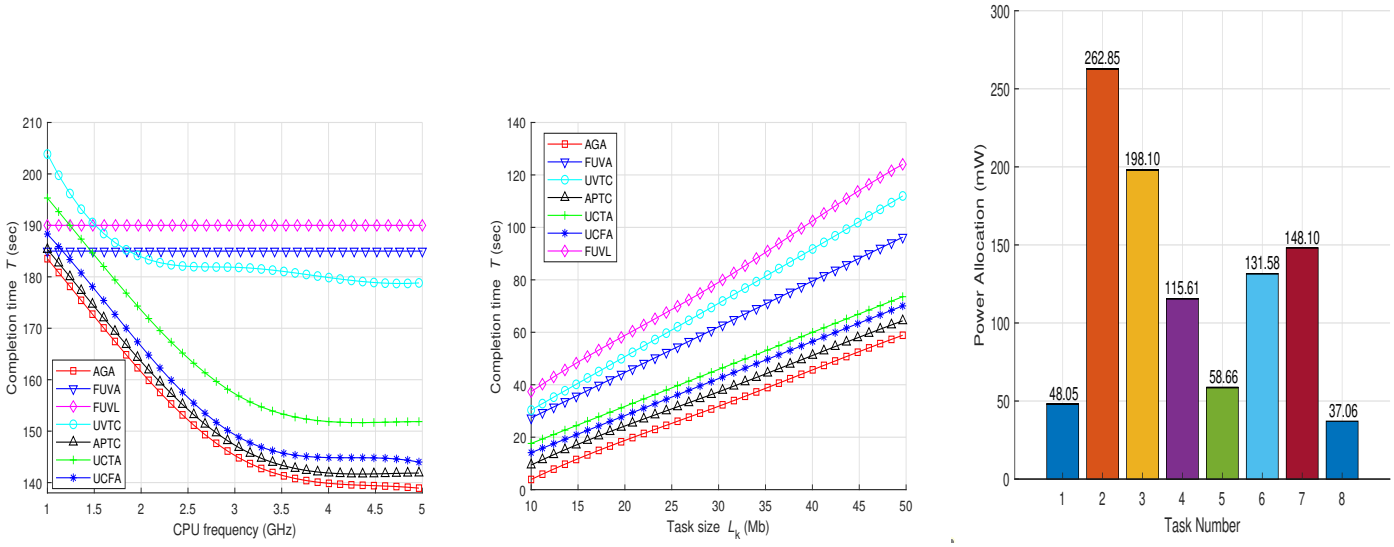

(a) (b) (c)

Fig. 3: (a) Completion time versus CPU frequency (b) Completion time versus task size (c) Power allocation versus different tasks.

A. Execution Time and Convergence Analysis

Firstly, we compare **Algorithm 1**-**3** in terms of execution time (sec) for achieving required algorithmic precision ϵ, which shows the level of precision an algorithm can achieve to generate the desired results. As shown in Fig. 2(a), the execution time for both SCA-based **Algorithm 1** and AGA-based **Algorithm 2** is log-linear and linear, whereas for SES-based **Algorithm 3**, it is exponential. Moreover, AGA-based **Algorithm 2** has lowest execution time for achieving required precision. Thus, in terms of execution time and lowest time-complexity derived in previous section, **Algorithm 2** is our preferred approach for tackling **P0**. In this regard, for **Algorithm 2**, the values of the numbers of the crossover pairs is chosen as 10000, and the probability of mutation is 0.6. Now, we show the convergence analysis of **Algorithm 2** in Fig. 2(b), in mere ten iterations, **Algorithm 2** is able to minimize the completion time for different short task sizes, which further establishes its superiority compared with the other two aforementioned algorithms.

B. Fixed Benchmark Sub-Methods

Next, we design several fixed benchmark sub-methods using **Algorithm 2**, which are described as: 1) access point task computations (APTC), where as the name implies, tasks of the IoT devices are only computed at the AP side. 2) unmanned aerial vehicle task computations (UVTC), where the UAV is assumed to handle and perform all the task computations at its side. 3) fixed unmanned aerial vehicle altitude (FUVA), where the UAV's height is assumed to be fixed at $h_{fix.} = 200$ m. At this height, the UAV is able to successfully balance the sub-task relaying and offloading to the AP side. 4) uniform CPU

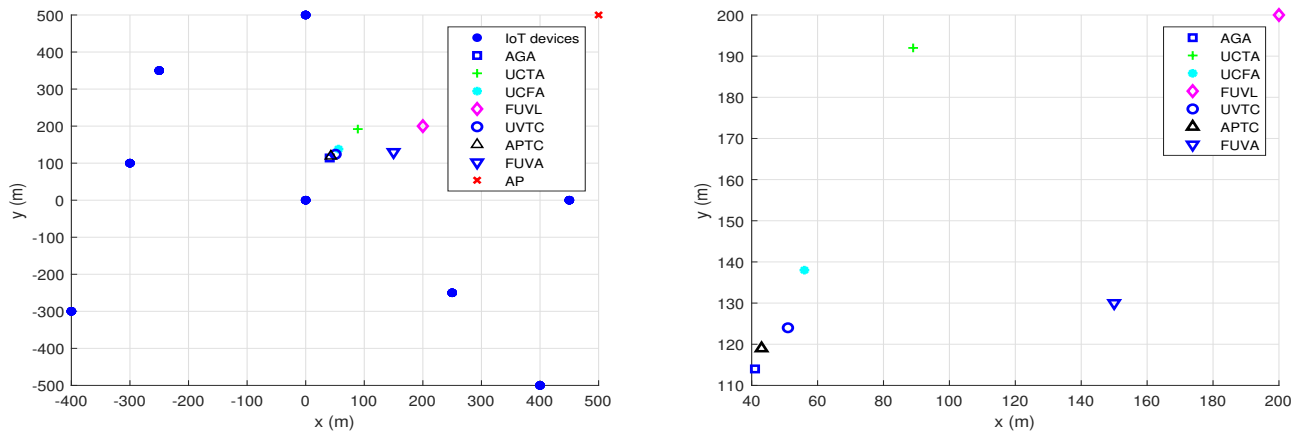

(a) (b)

Fig. 4: (a) 2D positioning of all devices (b) 2D UAV positioning using different fixed benchmark sub-methods

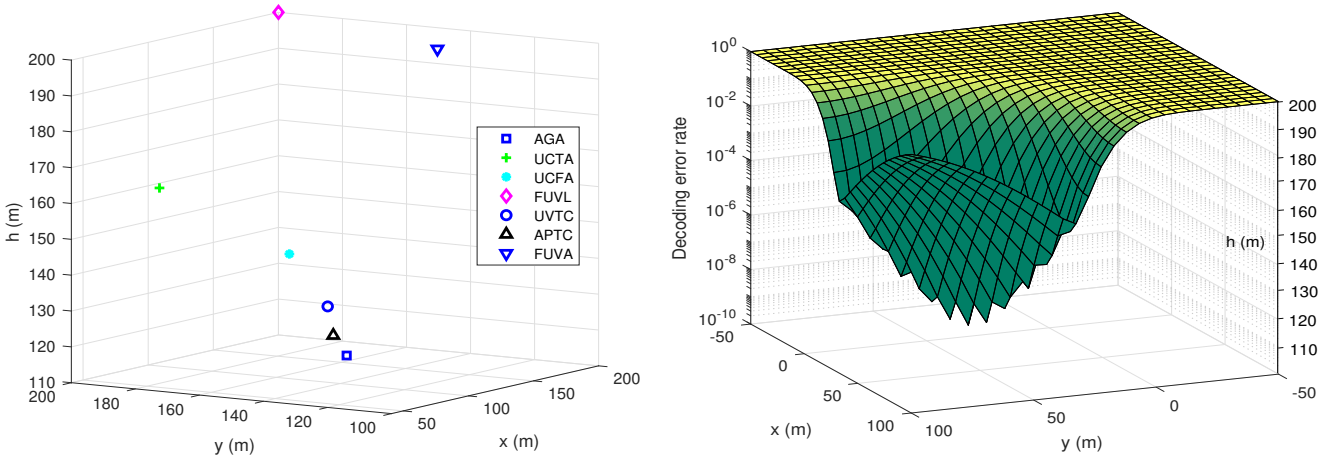

(a) (b)

Fig. 5: (a) 3D UAV positioning using different fixed benchmark sub-methods (b) 3D UAV positioning for decoding error rate.

frequency allocation (UCFA), where the resource allocation including CPU frequency of UAV is uniformly distributed; 5) uniform computational task assignment (UCTA), where the same number of tasks are calculated at both the UAV side as well as the AP side. 6) fixed unmanned aerial vehicle location (FUVL), where the UAV location is assumed to be fixed at the abscissa and ordinate of $u = [200, 200, 200]$ m.

C. Resource Allocation

Now, we evaluate the resource allocation including the UAV transmit power, UAV CPU frequency, communication bandwidth, blocklength, and task partitioning using our proposed AGA-based **Algorithm 2**, and its fixed benchmark sub-methods, which were described previously. Moreover, in Fig. 3(a), we show the relationship of completion time (sec) versus CPU frequency (GHz). It is abundantly clear that the AGA outperforms its fixed counterparts. Here, APTC yields comparable results to AGA, which emphasizes the significance of UAV relaying. It is to be noted that both FUVA and FUVL yield identical results, which remain constant by varying the value of F_{max}. In this regard, during the second phase, UAV to ground channel quality is adversely affected by UAV altitude and overall three-dimensional positioning, which stops the minimization of the completion time. Furthermore, Fig. 3(b) shows that completion time increases almost linearly as task size L_k tends to increase. In this context, yet again AGA-based **Algorithm 2** yields the best results compared to other benchmark sub-methods. Since FUVA and FUVL have fixed positioning they are ineffective in reducing the completion time. Additionally, APTC depicts the significance of task relaying to the remote AP, which conclusively show that if UAV is used to store and execute a sub-task while relaying the other sub-task to the remote AP, the best results can be obtained. Hence, it is essential to jointly optimize resource allocation including UAV transmit power, bandwidth, as well as task partitioning. Thereafter, Fig. 3(c) shows power allocation (mW) for different computation tasks at the UAV side. Moreover, for the power allocation process, the sum of

power levels of all tasks can only be up to the maximum UAV transmit power, which is set to 1000 mW or 30 dBm. As such, power differentiation between different computation tasks is random, which adds an extra layer of against the eavesdroppers. Resultantly, intercepting and decoding such task data packets become more difficult as eavesdroppers need to constantly adapt their equipment to account for the varying power levels and potential changes in the power allocation scheme.

D. UAV Positioning

Now, again we evaluate the different UAV deployment scenarios and decoding error rate using our proposed AGA-based **Algorithm 2**, and its fixed benchmark sub-methods, which were described previously. In this regard. Fig. 4(a) shows the positioning of all the devices including UAV, IoT devices, as well as AP. Moreover, Fig. 4(b) and Fig. 5(a), show the two-dimensional and three-dimensional positioning of the UAV using AGA and its sub-methods, as expected the optimal results are yielded by AGA and then second best results are yielded by APTC, which indicates that if UAV does not have storage and computational capabilities, i.e., buffer then it can simply offload tasks to the AP side and it will provide us with sub-optimal results for the considered scenario. Alternatively, for FUVA and FUVL, as described earlier, since the UAV height and 3D positioning are fixed, respectively, their deployment results are not ideal. Comparably, UCTA and UCFA produce better results than FUVA and FUVL, indicating that height and positioning are essential for determining optimal UAV deployment compared to other parameters like CPU frequency, which intuitively makes sense. Therefore, for all the benchmark sub-methods, we can positively deduce that they produce inferior results for UAV deployment compared to the AGA-based **Algorithm 2**. Finally, in Fig. 5(b), we show the relationship between decoding error error and the 3D positioning of the UAV, when UAV is deployed between the IoT devices and the AP. In this regard, we show that using our AGA-based **Algorithm 2**, subject to the 3D positioning of the UAV, the decoding error rate can be effectively reduced as UAV tries to balance the scales between task relaying and execution at its end.

VI. Conclusion

In this paper, we proposed a novel framework to facilitate URLLC vis-à-vis UAV-enabled relaying in MEC systems for 6g networks in uplink transmissions under short blocklength regime. Thereafter, we formulated the minimization problem of mission completion time subject to the constraints of resource allocation including UAV transmit power, UAV CPU frequency, communication bandwidth, task partitioning, decoding error rate and 3D UAV positioning. Afterwards, we proposed three distinct optimization algorithms and based on the lower time-complexity, as well as lower execution and convergence time, we selected AGA as the winning candidate. In this regard, AGA yielded superior performance compared to its fixed benchmark sub-methods and we demonstrated through simulations that it can successfully perform the resource allocation of the aforementioned constraints and can map 3D UAV positioning. Lastly, we showed that 3D UAV positioning is essential to reduce decoding error rate to meet QoS requirements for URLLC services. In our future work, we will explore the combination of power allocation with advanced physical layer security techniques to enhance data confidentiality and mitigate information leakage risks in UAV communications. By integrating adaptive modulation and coding, beamforming, and interference management with power allocation, we aim to achieve a higher level of security for transmitted data. These techniques will dynamically adapt to channel conditions, optimize resource allocation, and address potential vulnerabilities, ensuring robust and secure UAV communication systems in diverse environments. Our research will contribute to the development of more secure and reliable communication systems for future UAV applications.

VII. Acknowledgement

This work was supported by Mitacs/Ultra Intelligence and Communications through project IT25839 and by the National Natural Sciences and Engineering Research Council of Canada (NSERC) under Grant RGPIN-2020-06050.

Appendix A
Convexity of $f(x_k, y_k)$

To show the convexity, we first show the right hand side of eq. (33c), as a mathematical function given by

$$f(x_k, y_k) = A_{k1}\ y_k^{-\alpha/2} + A_{k2}\ x_k^{-1}\ y_k^{-\alpha/2}, \tag{40}$$

For the sake of simplicity, we substitute the value of $\alpha = 2.3$, to simplify the eq. (40) as

$$f(x_k, y_k) = A_{k1}\ y_k^{-1.15} + A_{k2}\ x_k^{-1}\ y_k^{-1.15}, \tag{41}$$

Now, the *Hessian matrix* of a two-variable function is a 2×2 square matrix of second-order partial derivatives shown by

$$\mathbf{H}(f(x_k, y_k)) = \begin{bmatrix} \dfrac{\partial^2 f(x_k, y_k)}{\partial x_k^2} & \dfrac{\partial^2 f(x_k, y_k)}{\partial x_k\, \partial y_k} \\ \dfrac{\partial^2 f(x_k, y_k)}{\partial y_k\, \partial x_k} & \dfrac{\partial^2 f(x_k, y_k)}{\partial y_k^2} \end{bmatrix}, \tag{42}$$

Afterwards, the general form of *Hessian matrix* can be given by

$$\mathbf{H}(f(x_k, y_k)) = \begin{bmatrix} \mathbf{H_{11}} & \mathbf{H_{12}} \\ \mathbf{H_{21}} & \mathbf{H_{22}} \end{bmatrix}, \tag{43}$$

where H_{ij} represent the corresponding elements of the matrix, as such i denotes the row index and j denotes the column index. Moreover, first element and second elements H_{11} and H_{12} can be computed as

$$\begin{aligned} \mathbf{H_{11}} &= \frac{\partial^2 f(x_k, y_k)}{\partial x_k^2} = \frac{2A_{k2}}{x_k^3 y_k^{1.15}}, \\ \mathbf{H_{12}} &= \frac{\partial^2 f(x_k, y_k)}{\partial x_k \partial y_k} = \frac{1.15A_{k2}}{x_k^2 y_k^{2.15}}. \end{aligned} \tag{44}$$

Thereafter, the third and the last elements denoted by H_{21} and H_{22} are calculated as

$$\begin{aligned}\mathbf{H_{21}} &= \frac{\partial^2 f(x_k,y_k)}{\partial y_k \partial x_k} = \frac{1.15A_{k2}}{x_k^2 y_k^{2.15}},\\ \mathbf{H_{22}} &= \frac{\partial^2 f(x_k,y_k)}{\partial x_k^2} = \frac{2.4725}{y_k^{3.15}}\left(A_{k1}+\frac{A_{k2}}{x_k}\right).\end{aligned} \tag{45}$$

It is to be noted that $H_{12} = H_{21}$, due to symmetric nature of the *Hessian matrix*. Here, we put all the computed matrix elements in eq. (42), and we get

$$\mathbf{H}(f(x_k,y_k)) = \begin{bmatrix} \frac{2A_{k2}}{x_k^3 y_k^{1.15}} & \frac{1.15A_{k2}}{x_k^2 y_k^{2.15}} \\ \frac{1.15A_{k2}}{x_k^2 y_k^{2.15}} & \frac{2.4725}{y_k^{3.15}}\left(A_{k1}+\frac{A_{k2}}{x_k}\right)\end{bmatrix}, \tag{46}$$

Furthermore, we compute the first-order and the second-order principal minors of $\mathbf{H}(f(x_k,y_k))$, given as

$$\Delta_1 = \mathbf{H_{11}} = \frac{2A_{k2}}{x_k^3 y_k^{1.15}}, \tag{47}$$

$$\Delta_2 = det\begin{bmatrix}\mathbf{H_{11}} & \mathbf{H_{12}} \\ \mathbf{H_{21}} & \mathbf{H_{22}}\end{bmatrix} = \frac{2.4725A_{k2}}{x_k^3 y_k^{4.3}}\left(2A_{k1}+\frac{1.4651A_{k2}^2}{x_k}\right), \tag{48}$$

Since, $\Delta_1 > 0$ and $\Delta_2 > 0$, it indicates that all the principal minors are positive. Thus, according to *Sylvester's criterion*, $\mathbf{H}(f(x_k,y_k))$ is positive semi-definite and it is convex in nature [45]–[48].

Appendix B
Convexity of $u_k((\mathbf{h}^j)^2 + \|\mathbf{q}^j - \mathbf{w}_k\|^2)$

Now, we show the convexity of elevation angle u_k w.r.t. distance $(\mathbf{h}^j)^2 + \|\mathbf{q}^j - \mathbf{w}_k\|^2$. As such, the first-order partial derivative of u_k w.r.t. $(\mathbf{h}^j)^2 + \|\mathbf{q}^j - \mathbf{w}_k\|^2$ is given as

$$\frac{\partial u_k}{\partial (\mathbf{h}^j)^2 + \|\mathbf{q}^j - \mathbf{w}_k\|^2} = \frac{-\mathbf{h}^j((\mathbf{h}^j)^2 + \|\mathbf{q}^j - \mathbf{w}_k\|^2)^{-1}}{2\sqrt{\|\mathbf{q}^j - \mathbf{w}_k\|^2}}, \tag{49}$$

Afterwards, we again compute the second-order partial derivative of u_k w.r.t. $(\mathbf{h}^j)^2 + \|\mathbf{q}^j - \mathbf{w}_k\|^2$, given as

$$\frac{\partial^2 u_k}{\partial ((\mathbf{h}^j)^2 + \|\mathbf{q}^j - \mathbf{w}_k\|^2)^2} = \frac{\mathbf{h}^j((\mathbf{h}^j)^2 + \|\mathbf{q}^j - \mathbf{w}_k\|^2)^{-2}}{2\sqrt{\|\mathbf{q}^j - \mathbf{w}_k\|^2}}, \tag{50}$$

Since, $\dfrac{\partial u_k}{\partial (\mathbf{h}^j)^2 + \|\mathbf{q}^j - \mathbf{w}_k\|^2} > 0$, thus, according to the second derivative test, the elevation angle u_k is convex w.r.t. $(\mathbf{h}^j)^2 + \|\mathbf{q}^j - \mathbf{w}_k\|^2$. Finally, the same principle applies to the convexity of u_k^2 w.r.t. $(\mathbf{h}^j)^2 + \|\mathbf{q}^j - \mathbf{w}_k\|^2$.

Appendix C
Convexity of $u_k(\mathbf{h})$

Again, we perform the convexity analysis of elevation angle u_k w.r.t. the UAV height $\mathbf{h}$. Same as before, the first-order partial derivative of u_k w.r.t. $\mathbf{h}$ is given as

$$\frac{\partial u_k}{\partial \mathbf{h}} = \frac{1}{\sqrt{\|\mathbf{q}^j - \mathbf{w}_k\|^2}}\Big\{1 - (\mathbf{h}^j)^2((\mathbf{h}^j)^2 + \|\mathbf{q}^j - \mathbf{w}_k\|^2)^{-1}\Big\}. \tag{51}$$

Similarly, once more we calculate the second-order partial derivative of u_k w.r.t. $\mathbf{h}$, given as

$$\begin{aligned}\frac{\partial^2 u_k}{\partial \mathbf{h}^2} =& \frac{1}{\sqrt{\|\mathbf{q}^j - \mathbf{w}_k\|^2}} + \frac{2\mathbf{h}^j((\mathbf{h}^j)^2 + \|\mathbf{q}^j - \mathbf{w}_k\|^2)^{-1}}{\sqrt{\|\mathbf{q}^j - \mathbf{w}_k\|^2}} \\ & \Big\{1 - (\mathbf{h}^j)^2((\mathbf{h}^j)^2 + \|\mathbf{q}^j - \mathbf{w}_k\|^2)^{-1}\Big\},\end{aligned} \tag{52}$$

Since, $\dfrac{\partial^2 u_k}{\partial \mathbf{h}^2} > 0$, therefore, yet again, according to the second derivative test, the elevation angle u_k is convex w.r.t. $\mathbf{h}$. Lastly, using the same convexity rule u_k^2 is also convex w.r.t. $\mathbf{h}$.

References

[1] J. C.-W. Lin, G. Srivastava, Y. Zhang, Y. Djenouri, and M. Aloqaily, "Privacy-preserving multiobjective sanitization model in 6g iot environments," *IEEE Internet Things J.*, vol. 8, no. 7, pp. 5340–5349, 2020.

[2] X. Xu, B. Shen, S. Ding, G. Srivastava, M. Bilal, M. R. Khosravi, V. G. Menon, M. A. Jan, and M. Wang, "Service offloading with deep q-network for digital twinning-empowered internet of vehicles in edge computing," *IEEE Trans. Ind. Informat.*, vol. 18, no. 2, pp. 1414–1423, 2020.

[3] M. M. Azari, S. Solanki, S. Chatzinotas, O. Kodheli, H. Sallouha, A. Colpaert, J. F. M. Montoya, S. Pollin, A. Haqiqatnejad, A. Mostaani *et al.*, "Evolution of non-terrestrial networks from 5g to 6g: A survey," *IEEE Commun. Surveys Tuts.*, 2022.

[4] Y. Zeng, R. Zhang, and T. J. Lim, "Wireless communications with unmanned aerial vehicles: Opportunities and challenges," *IEEE Commun. Mag.*, vol. 54, no. 5, pp. 36–42, 2016.

[5] P. S. Bithas, E. T. Michailidis, N. Nomikos, D. Vouyioukas, and A. G. Kanatas, "A survey on machine-learning techniques for uav-based communications," *Sensors*, vol. 19, no. 23, p. 5170, 2019.

[6] H. Nawaz, H. M. Ali, and A. A. Laghari, "Uav communication networks issues: a review," *Arch. Comput. Meth. Eng.*, vol. 28, no. 3, pp. 1349–1369, 2021.

[7] J. Zhao, F. Gao, G. Ding, T. Zhang, W. Jia, and A. Nallanathan, "Integrating communications and control for uav systems: Opportunities and challenges," *IEEE Access*, vol. 6, pp. 67 519–67 527, 2018.

[8] B. Li, Z. Fei, Y. Zhang, and M. Guizani, "Secure uav communication networks over 5g," *IEEE Wireless Commun.*, vol. 26, no. 5, pp. 114–120, 2019.

[9] X. Ma, Z. Na, B. Lin, and L. Liu, "Energy efficiency optimization of uav-assisted wireless powered systems for dependable data collections in internet of things," *IEEE Trans. Rel.*, 2022.

[10] A. A. Khuwaja, Y. Chen, N. Zhao, M.-S. Alouini, and P. Dobbins, "A survey of channel modeling for uav communications," *IEEE Commun. Surv. Tuts.*, vol. 20, no. 4, pp. 2804–2821, 2018.

[11] H. Wang, J. Wang, J. Chen, Y. Gong, and G. Ding, "Network-connected uav communications: Potentials and challenges," *China Commun.*, vol. 15, no. 12, pp. 111–121, 2018.

[12] Y. Zeng, Q. Wu, and R. Zhang, "Accessing from the sky: A tutorial on uav communications for 5g and beyond," *in Proc. IEEE*, vol. 107, no. 12, pp. 2327–2375, 2019.

[13] B. Hu and X. Dong, "Communications channel characteristics due to aircraft body blockage in urban air mobility," *IEEE Commun. Lett.*, 2022.

[14] R. Zhang, R. Tang, Y. Xu, and X. Shen, "Resource allocation for uav-assisted noma systems with dual connectivity," *IEEE Wireless Commun. Lett.*, 2022.

[15] V. U. Pai and B. Sainath, "Uav selection and link switching policy for hybrid tethered uav-assisted communication," *IEEE Commun. Lett.*, vol. 25, no. 7, pp. 2410–2414, 2021.

[16] Z. Liu, G. Huang, Q. Zhong, H. Zheng, and S. Zhao, "Uav-aided vehicular communication design with vehicle trajectory's prediction," *IEEE Wireless Commun. Lett.*, vol. 10, no. 6, pp. 1212–1216, 2021.

[17] C. Zhong, J. Yao, and J. Xu, "Secure uav communication with cooperative jamming and trajectory control," *IEEE Commun. Lett.*, vol. 23, no. 2, pp. 286–289, 2018.

[18] Z. Wang and J. Zheng, "Rate meta distribution of downlink base station cooperation for cellular-connected uav networks," *IEEE Commun. Lett.*, 2022.

[19] W. Xie, Y. Li, C. Yu, J. Wang, X. Peng, and P. Zhu, "Sum rate maximization for self-sustainable irs-assisted uav communications," *IEEE Commun. Lett.*, 2022.

[20] B. Liu, Y. Wan, F. Zhou, Q. Wu, and R. Q. Hu, "Resource allocation and trajectory design for miso uav-assisted mec networks," *IEEE Trans. Veh. Technol.*, 2022.

[21] Y. Nie, J. Zhao, F. Gao, and F. R. Yu, "Semi-distributed resource management in uav-aided mec systems: A multi-agent federated reinforcement learning approach," *IEEE Trans. Veh. Technol.*, vol. 70, no. 12, pp. 13 162–13 173, 2021.

[22] L. Sun, L. Wan, and X. Wang, "Learning-based resource allocation strategy for industrial iot in uav-enabled mec systems," *IEEE Trans. Ind. Informat.*, vol. 17, no. 7, pp. 5031–5040, 2020.

[23] Z. Hu, F. Zeng, Z. Xiao, B. Fu, H. Jiang, and H. Chen, "Computation efficiency maximization and qoe-provisioning in uav-enabled mec communication systems," *IEEE Trans. Net. Sci. Eng.*, vol. 8, no. 2, pp. 1630–1645, 2021.

[24] C. Zhan, H. Hu, X. Sui, Z. Liu, and D. Niyato, "Completion time and energy optimization in the uav-enabled mobile-edge computing system," *IEEE Internet Things J.*, vol. 7, no. 8, pp. 7808–7822, 2020.

[25] M. Elwekeil, A. Zappone, and S. Buzzi, "Power control in cell-free massive mimo networks for uavs urllc under the finite blocklength regime," *IEEE Trans. Commun.*, 2022.

[26] Y. Ji, K. Yu, J. Qiu, and J. Yu, "Massive mimo and secrecy guard zone based improving physical layer security in uav-enabled urllc networks," *IEEE Trans. Veh. Technol.*, 2022.

[27] X. Xi, X. Cao, P. Yang, J. Chen, T. Q. Quek, and D. Wu, "Network resource allocation for embb payload and urllc control information communication multiplexing in a multi-uav relay network," *IEEE Trans. Commun.*, vol. 69, no. 3, pp. 1802–1817, 2020.

[28] A. Ranjha, G. Kaddoum, and K. Dev, "Facilitating urllc in uav-assisted relay systems with multiple-mobile robots for 6g networks: A prospective of agriculture 4.0," *IEEE Trans. Ind. Informat.*, vol. 18, no. 7, pp. 4954–4965, 2021.

[29] A. Ranjha and G. Kaddoum, "Urllc-enabled by laser powered uav relay: A quasi-optimal design of resource allocation, trajectory planning and energy harvesting," *IEEE Trans. Veh. Technol.*, vol. 71, no. 1, pp. 753–765, 2021.

[30] A. Ranjha, G. Kaddoum, M. Rahim, and K. Dev, "Urllc in uav-enabled multicasting systems: A dual time and energy minimization problem using uav speed, altitude and beamwidth," *Comput. Commun.*, vol. 187, pp. 125–133, 2022.

[31] X. Sun, D. W. K. Ng, Z. Ding, Y. Xu, and Z. Zhong, "Physical layer security in uav systems: Challenges and opportunities," *IEEE Wireless Commun.*, vol. 26, no. 5, pp. 40–47, 2019.

[32] M. Chiang, P. Hande, T. Lan, C. W. Tan *et al.*, "Power control in wireless cellular networks," *Foundations and Trends® in Networking*, vol. 2, no. 4, pp. 381–533, 2008.

[33] M. Bennis, M. Debbah, and H. V. Poor, "Ultrareliable and low-latency wireless communication: Tail, risk, and scale," *in Proc. IEEE*, vol. 106, no. 10, pp. 1834–1853, Sep. 2018.

[34] L. Bariah, L. Mohjazi, S. Muhaidat, P. C. Sofotasios, G. K. Kurt, H. Yanikomeroglu, and O. A. Dobre, "A prospective look: Key enabling technologies, applications and open research topics in 6g networks," *IEEE Access*, vol. 8, pp. 174 792–174 820, 2020.

[35] C. She, C. Sun, Z. Gu, Y. Li, C. Yang, H. V. Poor, and B. Vucetic, "A tutorial on ultrareliable and low-latency communications in 6g: integrating domain knowledge into deep learning," *Proc. IEEE*, vol. 109, no. 3, pp. 204–246, 2021.

[36] Y. Liu, X. Ma, L. Shu, G. P. Hancke, and A. M. Abu-Mahfouz, "From industry 4.0 to agriculture 4.0: Current status, enabling technologies, and research challenges," *IEEE Trans. Ind. Informat.*, vol. 17, no. 6, pp. 4322–4334, 2020.

[37] C. You and R. Zhang, "3d trajectory optimization in rician fading for uav-enabled data harvesting," *IEEE Trans. Wireless Commun.*, vol. 18, no. 6, pp. 3192–3207, 2019.

[38] Y. Polyanskiy, H. V. Poor, and S. Verdú, "Channel coding rate in the finite blocklength regime," *IEEE Trans. Inf. Theory*, vol. 56, no. 5, pp. 2307–2359, Apr. 2010.

[39] Y. Xu, T. Zhang, D. Yang, Y. Liu, and M. Tao, "Joint resource and trajectory optimization for security in uav-assisted mec systems," *IEEE Trans. Commun.*, vol. 69, no. 1, pp. 573–588, 2020.

[40] Y. Xu, T. Zhang, D. Yang, and L. Xiao, "Uav-assisted relaying and mec networks: Resource allocation and 3d deployment," in *IEEE Int. Conf. Commun. Workshops (ICC Workshops)*. IEEE, 2021, pp. 1–6.

[41] T. Zhang, Y. Xu, J. Loo, D. Yang, and L. Xiao, "Joint computation and communication design for uav-assisted mobile edge computing in iot," *IEEE Trans. Ind. Informat.*, vol. 16, no. 8, pp. 5505–5516, 2019.

[42] H. Ren, C. Pan, K. Wang, Y. Deng, M. Elkashlan, and A. Nallanathan, "Achievable data rate for urllc-enabled uav systems with 3-d channel model," *IEEE Wireless Commun. Lett.*, vol. 8, no. 6, pp. 1587–1590, 2019.

[43] S. Bubeck *et al.*, "Convex optimization: Algorithms and complexity," *Foundations and Trends® in Machine Learning*, vol. 8, no. 3-4, pp. 231–357, 2015.

[44] T. Wang and L. Vandendorpe, "Successive convex approximation based methods for dynamic spectrum management," in *IEEE Int. Conf. Commun. (ICC)*. IEEE, 2012, pp. 4061–4065.

[45] S. Boyd, S. P. Boyd, and L. Vandenberghe, *Convex optimization*. Cambridge university press, 2004.

[46] D. Bertsekas, *Convex optimization theory*. Athena Scientific, 2009, vol. 1.

[47] A. Ben-Tal and A. Nemirovski, "Robust convex optimization," *Mathematics of operations research*, vol. 23, no. 4, pp. 769–805, 1998.

[48] Z.-Q. Luo and W. Yu, "An introduction to convex optimization for communications and signal processing," *IEEE J. Sel. Areas Commun.*, vol. 24, no. 8, pp. 1426–1438, 2006.

Ali Ranjha received his Ph.D. degree in Engineering from the École de Technologie Supérieure (ÉTS), Université du Québec, Montréal, Canada, where he is also presently working as a postdoctoral researcher. His research interests include fundamental communication theory, UAV communications, Internet of Things (IoT), URLLC, and optimization in resource-constrained networks.

Diala Naboulsi (Member, IEEE) received her Ph.D. degree in computer science from INSA Lyon in 2015. She is an Associate Professor with the École de Technologie Supérieure (ÉTS), Canada. Before that, she held a Research Professional position with the Ultra-TCS Research Chair, ÉTS and a Research Associate position and a Postdoctoral Researcher position with Concordia University, Canada. Her research interests are in mobile networks, virtualized networks, and wireless networks.

Mohamed El Emary is working towards his Ph.D. degree in Engineering at École de Technologie Supérieure (ÉTS), Canada. His research interests are mobile edge computing in UAV networks using optimization and Machine Learning approaches.

Francois Gagnon (Senior Member, IEEE) received the B.Eng. and Ph.D. degrees in Electrical Engineering from the École Polytechnique de Montréal. He has been a Professor with the Department of Electrical Engineering, École de technologie supérieure (ÉTS), since 1991, where he served as the Director, from 1999 to 2001, and has held the industrial research chair position, since 2001. He is also the NSERC-Ultra Electronics Chair in Wireless Emergency and Tactical Communication, the most prestigious industrial chair program in Canada. He also founded the Communications and Microelectronic Integration Laboratory at the ETS, and was its first Director. Most recently, he was appointed as the Director General of ÉTS in June 2019. His research interests include wireless communications, modulation, coding, microelectronics, signal processing, equalization, software-defined radio, mobile communication, and fading channels.